Journal of Food Engineering 99 (2010) 206–215

Contents lists available at ScienceDirect

Journal of Food Engineering

journal homepage: www.elsevier.com/locate/jfoodeng

Multifractal properties of pore-size distribution in apple tissue using X-ray imaging

Fernando Mendoza [a], Pieter Verboven [a], Quang Tri Ho [a], Greet Kerckhofs [b,1], Martin Wevers [b,1], Bart Nicolaï [a,*]

[a] BIOSYST – MeBioS, Faculty of Bioscience Engineering, Katholieke Universiteit Leuven, W. de Croylaan 42, BE-3001 Leuven, Belgium
[b] Materials Performance and Non-Destructive Evaluation, Department of Metallurgy and Materials Engineering (MTM), Katholieke Universiteit Leuven, Kastelpark Arenberg 44, BE-3001 Leuven, Belgium

ARTICLE INFO

Article history:
Received 30 April 2009
Received in revised form 16 February 2010
Accepted 19 February 2010
Available online 24 February 2010

Keywords:
Apple tissue
Generalized dimensions
Image analysis
Multifractal analysis
Pore-scale microstructure
Singularity spectrum
X-ray microtomography

ABSTRACT

The pore-size distribution (PSD) has an important influence on the complex gas transport phenomena (O_2 and CO_2) that occur in apple tissue during storage under controlled atmosphere conditions. It defines the apple tissue microstructure that is correlated to many other apple properties. In this article multifractal analysis (MFA) has been used to study the multiscale structure of the PSD using generalized dimensions in three varieties of apples (*Jonagold*, *Greenstar*, and *Kanzi*) based on X-ray imaging technology (8.5 μm resolution). Tomographic images of apple samples were taken at two positions within the parenchyma tissue: close to the peel and near to the core. The images showed suitable scaling properties. The generalized dimensions were determined with an R^2 greater than 0.98 in the range of moment orders between −1 and +10. The variation of D_q with respect to q and the shape of the multifractal generalized spectrum revealed that the PSD structure of apple tissue has properties close to multifractal self-similarity measures. Comparisons among cultivars showed that, in spite of the complexity and variability of the pore space of these apple samples, the extracted generalized dimensions from PSD were significantly different ($p < 0.05$). The generalized dimensions D_0, D_1, D_2, and the quantity D_0–D_2 could be used to discriminate tissue samples from different positions or cultivars. Also, high correlations were found between these parameters and the porosity ($R^2 \geqslant 0.935$). These results demonstrate that MFA is an appropriate tool for characterizing the internal pore-size distribution of apple tissue and thus may be used as a quantitative measure to understand how tissue microstructure affects important physical properties of apple.

1. Introduction

An apple fruit is mainly composed of the fleshy tissue of parenchyma cells permeated with vascular and intercellular air spaces (Esau, 1977), and the structural geometry of these intercellular spaces or porous media plays a fundamental role in fluid and gas transport through its tissue (Celia et al., 1995; Dražeta et al., 2004). In general, in plant organs the gas filled intercellular spaces are considered the predominant pathways for gas transport through the plant and are greatly related to the characteristics of gas exchange (Kuroki et al., 2004; Raven, 1996). The volume of air increases during fruit growth and occupies a considerable proportion of the fruit at harvest (Harker and Ferguson, 1988; Yamaki and Ino, 1992; De Smedt et al., 1998). This increase in air space is accompanied by a proportional decline in fruit density while the density of the fruit cells themselves remains roughly constant (Baoping, 1999; Westwood et al., 1967). In addition, the microstructure and porosity differs between cultivars and also between positions in the parenchyma tissue of the same fruit (Baumann and Henze, 1983; Vincent, 1989). Larger fruit of the same cultivar have a higher proportion of air than smaller ones (Volz et al., 2004). Therefore, the characterization of these intercellular air spaces and distribution based on microstructural properties is important for agricultural applications since this may improve our understanding of fruit physiology and postharvest quality of the fruit during preservation. Fruit with greater porosity have been shown to be softer (Volz et al., 2004; Yearsley et al., 1997a,b), or more mealy (Harker and Hallet, 1992; Tu et al., 1996) and to have greater internal gas diffusion rates (Ho et al., 2006; Rajapakse et al., 1990). Furthermore, the volume of these intercellular air spaces continues to increase during storage, and therefore, its measurement can be used to define the age of the fruit and also to characterize the effect of different storage conditions on its quality (Harker et al., 1999; Khan and Vincent, 1990; Tu et al., 1996). All these features could be related to its known susceptibility to controlled atmosphere related disorders such as core breakdown in Conference pear (Cheng et al., 1998; Franck et al., 2007; Ho et al., 2008, 2009; Verboven et al., 2008).

A quantitative description of the microstructural features of the fruit tissue is required to understand the postharvest behavior of apple fruit. Fractal analysis seems appropriate for this purpose. Fractal objects have a structure which is similar independent of

* Corresponding author. Tel.: +32 16 322375; fax: +32 16 322955.
E-mail address: Bart.Nicolai@biw.kuleuven.be (B. Nicolaï).
[1] Tel.: +32 16 321303; fax: +32 16 321990.

0260-8774/$ - see front matter © 2010 Elsevier Ltd. All rights reserved.
doi:10.1016/j.jfoodeng.2010.02.021

Nomenclature

D_q	generalized fractal dimensions for different values of q
D_0, D_1, D_2	capacity dimension, entropy dimension, and correlation dimension, respectively
$f(\alpha)$	fractal dimension of the set of boxes with singularities α (i.e. interval $[\alpha, \alpha + d\alpha]$)
$N(\alpha)$	number of boxes where the probability has values in the interval $[\alpha, \alpha + d\alpha]$
$N(\varepsilon)$	number of boxes of size ε which contain at least one pixel representing the object (pore space)
$N_i(\varepsilon)$	number of pixels in each box i of scale ε belonging to the measured object (pore space)
$p_i(\varepsilon)$	mass probability in each box i of scale ε of the measured object (pore space)
$X(q, \varepsilon)$	partition function based on the moments of order q in the distribution of probabilities $p_i(\varepsilon)$

Greek symbols

α_i	Lipschitz–Hölder exponent characterizing the density in the ith box
ε	spatial scale in pixels
τ_q	mass exponent of the qth order moment

the scale and are characterized by a non-integer (fractal) dimension. Many natural objects have a fractal geometry (Mandelbrot, 1989). Multifractal formalisms involve decomposing self-similar measures into intertwined fractal sets, which are characterized by their singularity strength and fractal dimension (Posadas et al., 2003). Multifractal characterization involves not a single dimension, but a sequence of generalized fractal dimensions. Thus, a combination of all the fractal sets produces a multifractal spectrum that characterizes the variability and heterogeneity of the studied variables (Kravchenko et al., 1999). The advantage of the multifractal approach is that multifractal parameters can be independent of the size of the studied objects (Cox and Wang, 1993), as well as that no assumption is required about the data following any specific distribution (Scheuring and Riedi, 1994).

Fractal analysis has been applied to describe ice crystals in frozen fruit (Hagiwara et al., 2002), potato tissue during heating in oil (Quevedo et al., 2002), blooming of chocolate (Quevedo et al., 2002), irregular color patterns during enzymatic browning of apple (Quevedo et al., 2009), fat crystal networks (Tang and Marangoni, 2008), microstructure of bread crumb (Gonzales-Barron and Butler, 2008) and of carrots and potato tissue during drying (Kerdpiboon et al., 2007). Multifractal analysis has been successfully applied to plant science, ecology and agronomy research to study vegetation patterns (Scheuring and Riedi, 1994), zooplankton biomass (Pascual et al., 1995), root system of legumes (Ketipearachchi and Tatsumi, 2000), spatial and temporal variability of residual soil NO_3–N and corn grain yield (Eghball et al., 2003), and soil structure under long-term wastewater irrigation (Xiaoyan et al., 2007) among others. However, very little information is available about the multifractality in plant fruits related to their macro- and microstructural properties.

We believe that the geometric characteristics of the pore-size distribution (PSD) in apples can be described well through the spectrum of local fractal dimensions. This hope is solidly based on the fact that such fractal approach provides multifractal outputs that might be adjusted in order to fit multifractal spectra obtained from experimental data. Furthermore, it is well known that deviation of local fractal dimensions is greater for non-uniform or natural plant structures (Dathe et al., 2006; Mandelbrot, 1989). Local fractal dimensions measured within a small region may, therefore, vary from point a point, and the object can be characterized better by a spectrum of fractal dimensions. Multifractal analysis may improve discrimination of apple microstructure with similar but delicately different morphology.

In this study, we applied multifractal analysis for determining multiscale properties of the PSD of apple tissue more precisely based on the computation of their spectrum of generalized dimensions extracted from 2-D cross-sections of tomographic images at 8.5 μm resolution. Further, we wanted to evaluate the potential of discriminating discriminate tissue samples from different positions or cultivars (cv. *Jonagold*, cv. *Greenstar*, and cv. *Kanzi*).

2. Theory of multifractal analysis

The starting point of the analysis is a 2-D binary image of the studied object or structure (in our case the pore space of apple parenchyma tissue). In a homogeneous fractal system, the measured object is assumed to have a structure which is repeated over different spatial scales. Thus, the number $N(\varepsilon)$ of features of certain size ε scale as (Chhabra and Jensen, 1989; Evertsz and Mandelbrot, 1992; Vicsek, 1992):

$$N(\varepsilon) \sim \varepsilon^{-D_0} \tag{1}$$

where D_0 is the fractal dimension describing the scaling properties or size distribution of two-dimensional objects, which is frequently expressed as:

$$D_0 = \lim_{\varepsilon \to 0} \frac{\log N(\varepsilon)}{\log \frac{1}{\varepsilon}} \tag{2}$$

The box-counting technique is used to obtain the scaling properties of 2-D fractal objects by covering the 2-D-image with a range of boxes of size ε and counting the number of boxes containing at least one pixel representing the object under study. This procedure is then repeated for a range of ε values and $D_0$is then calculated from Eq. (2). This means that the technique does not consider the amount of mass (density of pixels) inside each box (Posadas et al., 2003). For describing heterogeneous or non-uniform systems, however, it is necessary to resolve regions with a high or low density of mass. In practice, a way to quantify local densities is by estimating the mass probability in the ith box as:

$$p_i(\varepsilon) = N_i(\varepsilon)/N_T \tag{3}$$

where $N_i(\varepsilon)$ is the number of pixels containing mass in the ith box and N_T is the total mass of the system. Thus, for heterogeneous or non-uniform systems the probabilities in the ith box $p_i(\varepsilon)$ scale as:

$$p_i(\varepsilon) \sim \varepsilon^{\alpha_i} \tag{4}$$

where α_i is called the Lipschitz–Hölder exponent or singularity strength, characterizing the density in the ith box (Feder, 1988; Halsey et al., 1986). By singularity we mean the rapid changes in the mass probability values for a change in each local position of the system. Similar α_i values can be found at different positions i. Subsequently, the number of boxes $N(\alpha)$ where the p_i has singularity strengths between α and $\alpha + d\alpha$ is found to scale as (Chhabra and Jensen, 1989; Halsey et al., 1986):

$$N(\alpha) \sim \varepsilon^{-f(\alpha)} \quad (5)$$

where $f(\alpha)$ can be defined as the fractal dimension of the set of boxes with singularities α. The exponent α can take on values from the interval $[\alpha_{-\infty}, \alpha_{+\infty}]$, and $f(\alpha)$ is usually a single function with a maximum at $df(\alpha(q))/d\alpha(q) = 0$, where q is the moment order of the distribution. Thus, when $q = 0, f_{max}$ is equal to the box-counting or D_0 dimension (Gouyet, 1996; Viksec, 1992).Multifractal sets can also be characterized through the scaling of the qth order moments of p_i distributions in the form (Chhabra and Jensen, 1989; Korvin, 1992):

$$X(q,\varepsilon) = \sum_{i=1}^{N(\varepsilon)} p_i^q(\varepsilon) \sim \varepsilon^{(q-1)D_q} \quad (6)$$

where $\sum_{i=1}^{N(\varepsilon)} p_i^q(\varepsilon)$ represents the partition function $X(q,\varepsilon)$, and D_q represents the generalized dimensions of the qth order moments of a distribution (Hentchel and Procaccia, 1983; Chhabra and Jensen, 1989). Based on the work of Rényi (1995) D_q is defined from Eq. (6) as:

$$D_q = \frac{1}{q-1} \lim_{\varepsilon \to 0} \frac{\log \sum_{i=1}^{N(\varepsilon)} p_i^q(\varepsilon)}{\log \varepsilon} \quad (7)$$

The generalized dimension D_q is a monotone decreasing function for all real q values within the interval $[\alpha_{-\infty}, \alpha_{+\infty}]$. When $q < 0$, the partition function emphasizes regions in the distribution having less concentration of a measure, whereas the opposite is true for $q > 0$ (Chhabra and Jensen, 1989). The exponent in Eq. (6) is known as the mass or correlation exponent of the qth order moments, $\tau(q)$ (Halsey et al., 1986; Viksec, 1992):

$$\tau(q) = (q-1)D_q \quad (8)$$

According to Eq. (8), a linear relationship between $\tau(q)$ and q implies a single fractal system characterized by one scaling exponent (homogeneous fractal). On the other hand, variable slopes in $\tau(q)$ vs. q are indicative of a multifractal (heterogeneous) system (Machs et al., 1995). A special case of the latter is the bifractal distribution defined by two slopes dominating the$\tau(q)$ vs. q plot (Korvin, 1992).

The $f(\alpha)$ spectrum and the generalized dimensions D_q contain the same information, both characterizing the interwoven ensemble of fractal dimensions $f(\alpha_i)$. In each of the ith fractals, p_i scales with the Lipschitz–Hölder exponent α_i. The generalized dimensions for $q = 0$, $q = 1$ and $q = 2$ are known as the capacity dimension D_0, information dimension D_1, and correlation dimension D_2, respectively. The capacity dimension is independent of q and provides global (or average) information of the system since all boxes have a weight of unity (Voss, 1988). This means that D_0 is equal to the dimension of a monofractal (Eq. (2)). For $q = 1$ it can be derived from Eq. (7) that

$$D_1 = \lim_{\varepsilon \to 0} \frac{\sum_{i=1}^{N(\varepsilon)} p_i \log p_i}{\log \varepsilon} \quad (9)$$

D_1 is directly related to the information or Shannon entropy (Shannon and Weaver, 1949) which quantifies the degree of disorder present in a distribution. The numerator in Eq. (9) corresponds to the entropy of a probability distribution. It also describes the decrease in information content when the size of the boxes increases. This is one of the analogies between multifractals and statistical mechanics. For $q = 2$ the correlation dimension D_2 can be obtained as:

$$D_2 = \lim_{\varepsilon \to 0} \frac{\log \sum_{i=1}^{N(\varepsilon)} p_i^2}{\log \varepsilon} \quad (10)$$

D_2 is mathematically associated with the correlation function (Grassberger and Procaccia, 1983) and computes the correlation of measures contained in intervals of size ε. In other words, it describes the probability of finding pixels belonging to the object within a given distance when starting on a pixel belonging to object.Fractal dimensions for higher moments can be estimated according to Eq. (7). The plot of D_q for different values of q is called the generalized dimensional spectrum or Rényi spectrum. The relationship between $D_0, D_1,$ and D_2 is $D_2 \leq D_1 \leq D_0$, where the equality $D_0 = D_1 = D_2$ occurs only if the fractal is statistically or exactly self-similar and homogeneous (Korvin, 1992).

The measurements of multifractals are mainly the measurements of a statistical distribution, which is why the results yield useful information even if the underlying structure does not show a self-similar or self-affine behavior (Plotnick et al., 1996).

3. Materials and methods

3.1. Apple samples

Three varieties of apples (*Malus* × *domestica* Borkh.) for cultivars *Jonagold*, *Greenstar* and *Kanzi*, with ~7.5 cm diameter, were selected from a commercial orchard in Belgium and stored under controlled atmosphere conditions (0.8 °C, 2.5% CO_2, and 1% O_2) until used. For analysis, samples were taken in duplicate parallel to the medial axis of each fruit (0° and 180° around the fruit) at two different positions: near to the skin (*outer* tissue, ~7 mm from the skin) and near to the core (*inner* tissue, ~15 mm from the core center). Each sample was cut into a cylinder of 5 mm diameter and 2 cm length, and enclosed in a plastic tube to avoid dehydration.

3.2. Image acquisition and processing

The samples were scanned using a SkyScan 1072 high resolution desk-top X-ray micro-CT system, (SkyScan, Aartselaar, Belgium; http://www.skyscan.be), with a linear resolution of 8.5 μm by pixel, operating at a voltage of 63 kV, current of 156 μA, an exposure time of 8.4 s, and scanned over the interval 0°–180° using a 0.9° scan step. To account for the non-uniformities in the X-ray beam and non-uniform response of the CCD detector, the raw images were corrected for dark and white fields by taken the average of flat field correction references collected at the beginning of the experiment. The X-ray shadow projections of the 3-D object, digitalized as 1024 × 1024 pixels size, were processed using a mathematical back-projection procedure to obtain reconstructed cross-section images of linear attenuation coefficient values with 256 gradations (8-bit). Thus, a complete stack of 600 2-D cross-sections of grey images of the object with an 8.5 μm interslice distance was obtained from each scanned apple sample (i.e., scanned length: 600 slices × 8.5 μm = 5.1 mm). Then, from the middle part of the scanned region, a region-of-interest (ROI; with 256 × 256 pixels) of cross-section was extracted and subjected to image analysis.

In order to get binary images necessary for the consecutive MFA, the pores needed to be segmented at a certain threshold. However, the distinction among the void and solid phases in radiographic images of apple tissue are frequently not sharp (i.e., they do not shown a bimodal distribution due to peak overlap in the attenuation coefficient histogram (Mendoza et al., 2007), and therefore, dedicated segmentation algorithms need to be used to closely represent the pore structure in the images. In this study, the partition of apple tissue images into pores and cellular material was performed using the kriging based segmentation algorithm developed by Oh and Lindquist (1999). The algorithm is a non-parametric formulation able to analyze regions of uncertainty based on the estimation of the spatial covariance of the image in conjunction with indicator kriging to determine object edges (Mardia and Hainsworth, 1988). More details about the scanning

process and segmentation algorithm of radiographic apple tissue images can be found in Mendoza et al. (2007).

3.3. Generalized dimensional analysis of apple images

The multifractal analysis was carried out using a box-counting algorithm which estimates the probability of containing a pore (void) for every single box of sizes 2, 4, 8, 16, 32, 64, 128, and 256 , (i.e., in steps of 2^k, $1 < k < 8$). Doing this for images of size 256×256 pixels avoids artifacts which occur when boxes do not entirely cover the image at the borders. The generalized dimensions are obtained as the slope of the partition function over box size, both taken as logarithms (Eq. (7)). This method is known as the method of moments (Evertsz and Mandelbrot, 1992), as D_q is estimated for every moment q. Since the X-ray CT technique gave 600 cross-section images per apple sample, the average value of the computed multifractal parameters from each stack of images and repetition were reported and used in further analyses.

Image pre-processing to render stacks of 2-D square images of apple tissue and multifractal analysis were performed using the Image Processing Toolbox of MATLAB v7.0 (MathWorks, Inc., Natick, MA).

4. Results

4.1. Characteristics of the pore space of apple tissue

Fig. 1 shows representative radiographic images and their corresponding binary images extracted from the *outer* and *inner* positions of the parenchyma fruit of each apple cultivar. By comparing the images it is clear that the microstructure of the different cultivars appears to be similar; yet their gas diffusion properties are very different (Ho et al., 2010) There is, however, a clear difference between the microstructure of the inner and outer cortex of the fruit. Near the surface of the skin, the pores appear roughly spherical and do not show much orientation. Inwards, close to the core, the pores appear elongated and show some orientation. Also, differences (heterogeneity) in the bulk porosity distribution between cultivars are visually evident. ANOVA analysis of the average porosity confirmed the differences ($p < 0.05$) between regions as well as revealed a higher variability between images from *outer* tissue than those computed from *inner* tissue, as represented by their standard deviations (see Table 2). However, comparison of average porosities among pairs of apple samples did not reveal any statistical differences between *Jonagold* and *Greenstar* tissue samples from the *outer* parenchyma ($p \geqslant 0.05$). A number of authors have demonstrated the heterogeneity of the porosity distribution in apples through visual inspection using sophisticated microscopy techniques and by computation of bulk porosity measurements in different positions of the parenchyma tissue (Dražeta et al., 2004; Khan and Vincent, 1990); however, the complex distribution of the air spaces have shown that a single average geometric measurements from digital images are not sufficient to characterize the heterogeneity of pore distribution in the whole-matrix of the apple (Mendoza et al., 2006, 2007) and cannot describe all data in the whole-range of the PSD. In this article, the application of a multifractal technique was therefore attempted.

4.2. Multifractal analysis

Fig. 2 shows the estimated average partition functions $X(q, \varepsilon)$ for box sizes in the range of 2–256 pixels. In general, the partition

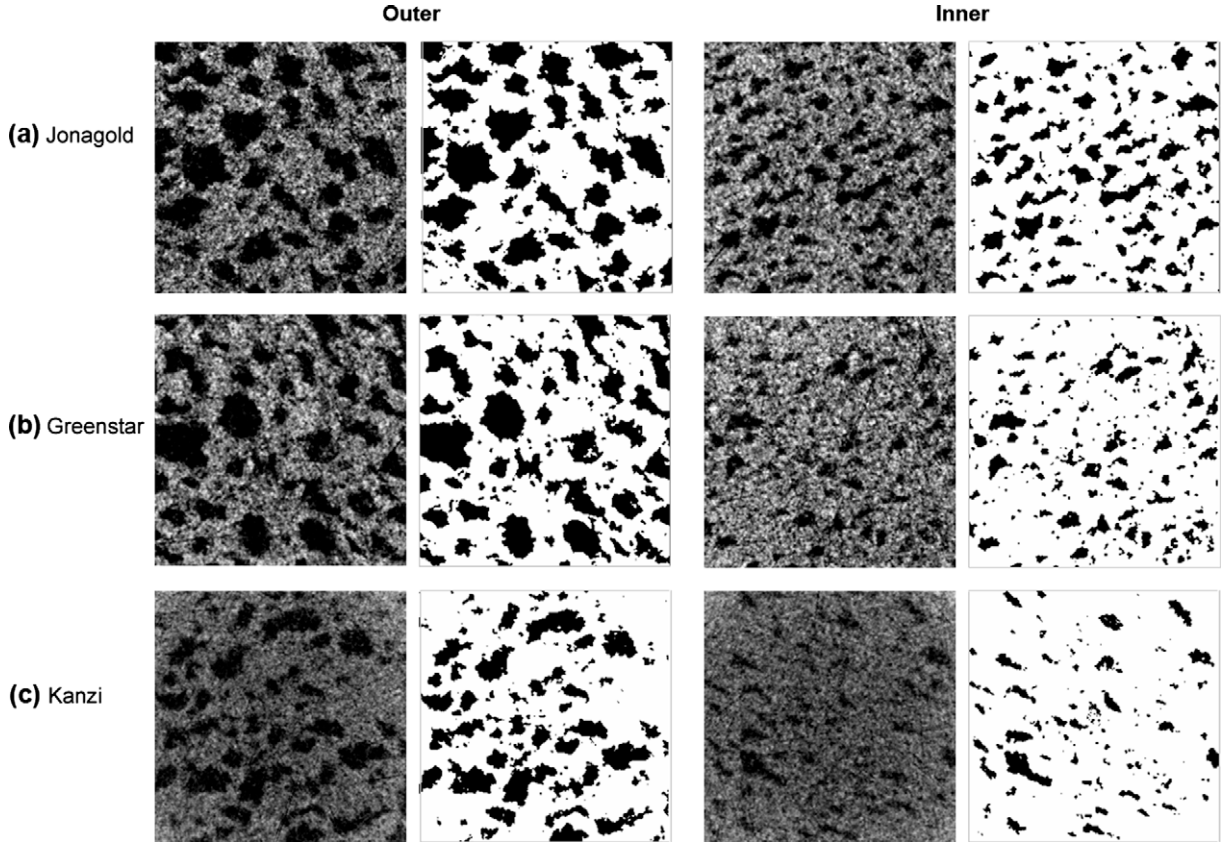

Fig. 1. Representative radiographic images and their corresponding binary images for *outer* (left) and *inner* (right) regions of parenchyma of apple tissue for cultivars *Jonagold* (a), *Greenstar* (b), and *Kanzi* (c). Black regions represent pores and grey regions represent cellular material. The binary images depict the efficiency of the kriging based segmentation algorithm according to Oh and Lindquist (1999).

Table 1
Average values of τ and their coefficients of determination (R^2), obtained for different values of q ($-10 \leqslant q \leqslant +10$).

q	Jonagold				Greenstar				Kanzi			
	Outer		Inner		Outer		Inner		Outer		Inner	
	$\tau(q)$	R^2	$\tau(q)$	R^2	$\tau(q)$	R^2	$\tau(q)$	R^2	$\tau(q)$	R^2	$\tau(q)$	R^2
−10	−23.85	0.885	−22.86	0.882	−23.85	0.879	−20.85	0.856	−23.12	0.861	−19.81	0.812
−9	−21.59	0.888	−20.70	0.885	−21.59	0.882	−18.90	0.859	−20.94	0.864	−17.97	0.816
−8	−19.34	0.891	−18.54	0.888	−19.33	0.885	−16.95	0.864	−18.75	0.868	−16.12	0.821
−7	−17.08	0.896	−16.38	0.892	−17.07	0.890	−14.99	0.869	−16.56	0.873	−14.27	0.827
−6	−14.82	0.901	−14.22	0.898	−14.81	0.895	−13.04	0.875	−14.37	0.879	−12.42	0.834
−5	−12.56	0.908	−12.06	0.905	−12.55	0.902	−11.09	0.883	−12.18	0.887	−10.57	0.844
−4	−10.30	0.918	−9.90	0.915	−10.29	0.913	−9.14	0.895	−10.00	0.898	−8.73	0.858
−3	−8.05	0.932	−7.75	0.929	−8.04	0.928	−7.19	0.912	−7.83	0.915	−6.88	0.879
−2	−5.84	0.955	−5.62	0.951	−5.83	0.951	−5.26	0.936	−5.69	0.942	−5.06	0.910
−1	−3.72	0.982	−3.58	0.977	−3.71	0.981	−3.38	0.965	−3.63	0.977	−3.27	0.953
0	−1.78	0.996	−1.71	0.992	−1.78	0.996	−1.62	0.984	−1.74	0.995	−1.57	0.984
1	0.00	–	0.00	–	0.00	–	0.00	–	0.00	–	0.00	–
2	1.72	0.999	1.64	0.997	1.72	0.999	1.53	0.994	1.69	0.999	1.49	0.996
3	3.43	0.999	3.25	0.997	3.44	0.999	3.02	0.995	3.37	0.999	2.94	0.997
4	5.13	0.999	4.85	0.997	5.14	0.999	4.49	0.995	5.04	0.999	4.38	0.997
5	6.83	0.999	6.45	0.997	6.85	0.999	5.95	0.995	6.71	0.998	5.82	0.997
6	8.54	0.998	8.04	0.997	8.56	0.998	7.41	0.995	8.38	0.998	7.25	0.996
7	10.24	0.998	9.64	0.997	10.27	0.998	8.86	0.995	10.06	0.998	8.67	0.996
8	11.94	0.998	11.23	0.997	11.98	0.998	10.32	0.995	11.73	0.998	10.10	0.996
9	13.65	0.998	12.83	0.997	13.69	0.998	11.77	0.995	13.41	0.998	11.53	0.995
10	15.35	0.998	14.42	0.996	15.40	0.998	13.22	0.995	14.31	0.998	12.95	0.995

Table 2
Results of the average generalized dimensions as well as the standard deviations and the corresponding R^2 of pore-size distributions of the studied apple cultivars for the first three positive moments q.

Cultivar	Region	Porosity	D_0	R^2	D_1	R^2	D_2	R^2	D_0-D_2	D_1/D_0
Jonagold	Outer	$0.292^{a} \pm 0.023$	$1.779^{a,\alpha} \pm 0.017$	0.996	$1.740^{a,\beta} \pm 0.018$	0.998	$1.723^{a,\gamma} \pm 0.018$	0.998	$0.056^{a} \pm 0.004$	$0.978^{a} \pm 0.002$
	Inner	$0.193^{b} \pm 0.019$	$1.708^{b,\alpha} \pm 0.023$	0.992	$1.660^{b,\beta} \pm 0.023$	0.996	$1.636^{b,\gamma} \pm 0.023$	0.997	$0.072^{b} \pm 0.004$	$0.972^{b} \pm 0.001$
Greenstar	Outer	$0.311^{a} \pm 0.030$	$1.777^{a,\alpha} \pm 0.023$	0.996	$1.740^{a,\beta} \pm 0.023$	0.998	$1.725^{a,\gamma} \pm 0.024$	0.999	$0.053^{c} \pm 0.004$	$0.979^{a} \pm 0.001$
	Inner	$0.108^{c} \pm 0.022$	$1.617^{c,\alpha} \pm 0.048$	0.984	$1.560^{c,\beta} \pm 0.049$	0.991	$1.527^{c,\gamma} \pm 0.050$	0.993	$0.090^{d} \pm 0.006$	$0.965^{c} \pm 0.002$
Kanzi	Outer	$0.255^{d} \pm 0.033$	$1.741^{d,\alpha} \pm 0.031$	0.995	$1.705^{d,\beta} \pm 0.031$	0.998	$1.690^{d,\beta} \pm 0.031$	0.999	$0.051^{e} \pm 0.005$	$0.979^{a} \pm 0.002$
	Inner	$0.090^{e} \pm 0.016$	$1.571^{e,\alpha} \pm 0.043$	0.984	$1.517^{e,\beta} \pm 0.043$	0.993	$1.487^{e,\gamma} \pm 0.043$	0.996	$0.083^{f} \pm 0.007$	$0.966^{c} \pm 0.003$

[a–f]Values with the same letters within each column indicate no significant differences among types of apple cultivars and parenchyma regions ($p \geqslant 0.05$).
[α,β,γ]Values with the same letters within each row indicate no significant differences among generalized dimensions D_0, and D_2 for each apple sample ($p \geqslant 0.05$).

functions of the apple pore space have similar shapes for all cultivars and sampled regions (*inner* and *outer* tissues) (see Fig. 2). For $q > 1$, the partition functions have positive slopes with a distinct linear behavior. For $q \leq 0$ the partition functions have a negative slope with a pronounced deviation from linearity for q moments equal or close to −10. The mass exponent τ was estimated according to Eq. (8) (shown in Table 1). The coefficients of determination (R^2) were smaller than 0.95 from $q < -2$ for both *outer* and *inner* tissue in *Jonagold* apples and *outer* tissue in *Greenstar*, and from $q < -1$ for *inner* tissue in *Greenstar* and for both *outer* and *inner* tissue in *Kanzi* apples. Nevertheless, over these order moments q, the correlations did not only improve when the q values increased; but also the differences of $\tau(q)$ increased between cultivars and, moreover, between *outer* and *inner* regions were compared. These significant differences in the mass exponent $\tau(q)$ give an indication of the inherent geometrical differences among apple pore microstructure, and consequently, among the PSD of the studied samples.

The corresponding Rényi spectra, D_q, for each apple cultivar in the range of moment order q between −10 and +10, as estimated from Eq. (8), are shown in Fig. 3. The generalized dimensions are sigma-shaped curves with a clear asymmetry with respect to the vertical axis and much more curvature for negative values of q than for positive ones where they are quasilinear. Specifically, they all exhibit pronounced decreasing D_q values with increasing q and reveal a similar behavior for *outer* tissue for *Jonagold* and *Greenstar* which also showed similar visual appearances of their pore-size distributions (Fig. 1) and no significant differences for their porosity estimations (see Table 2). The observed range of D_q was from $D_{-10} = 2.168 \pm 0.046$ (*Jonagold*) to $D_{+10} = 1.676 \pm 0.032$ (*Kanzi*) for *outer* tissue and from $D_{-10} = 2.078 \pm 0.041$ (*Greenstar*) to $D_{+10} = 1.439 \pm 0.045$ (*Kanzi*) for *inner* tissue. When the D_q values are close together this indicates a homogeneous structure; in a monofractal they are equal (i.e., constant D_q estimations). Analysis of the amplitude of D_q of each particular cultivar showed that in the *outer* tissue D_q is greater than in the *inner* one, which suggests that the heterogeneity of the PSD of the parenchyma tissue near the skin is larger than that of tissue near the core. Furthermore, it is evident from Fig. 3 that the Rényi spectra curves of the analyzed apple cultivars clearly confirm the observed visual differences in Fig. 1.

Detailed results for D_0, D_1 and D_2 can be found in Table 2, including the corresponding porosities and coefficients of determination (R^2) for each position and cultivar. The average values of the capacity dimension (D_0), entropy (D_1), and correlation (D_2) showed the same statistical differences when the apple regions and cultivars ($p < 0.05$) were compared. With the exception of the *outer* tissue for *Jonagold* and *Greenstar*, all the apple samples possessed a characteristic different dimension D_q in relation to their PSD. The coefficients of determination for these set of generalized dimensions (D_0, D_1 andD_2) were higher than 0.984 for all apple samples, and increased slightly with increasing q (Table 2). In addition, the

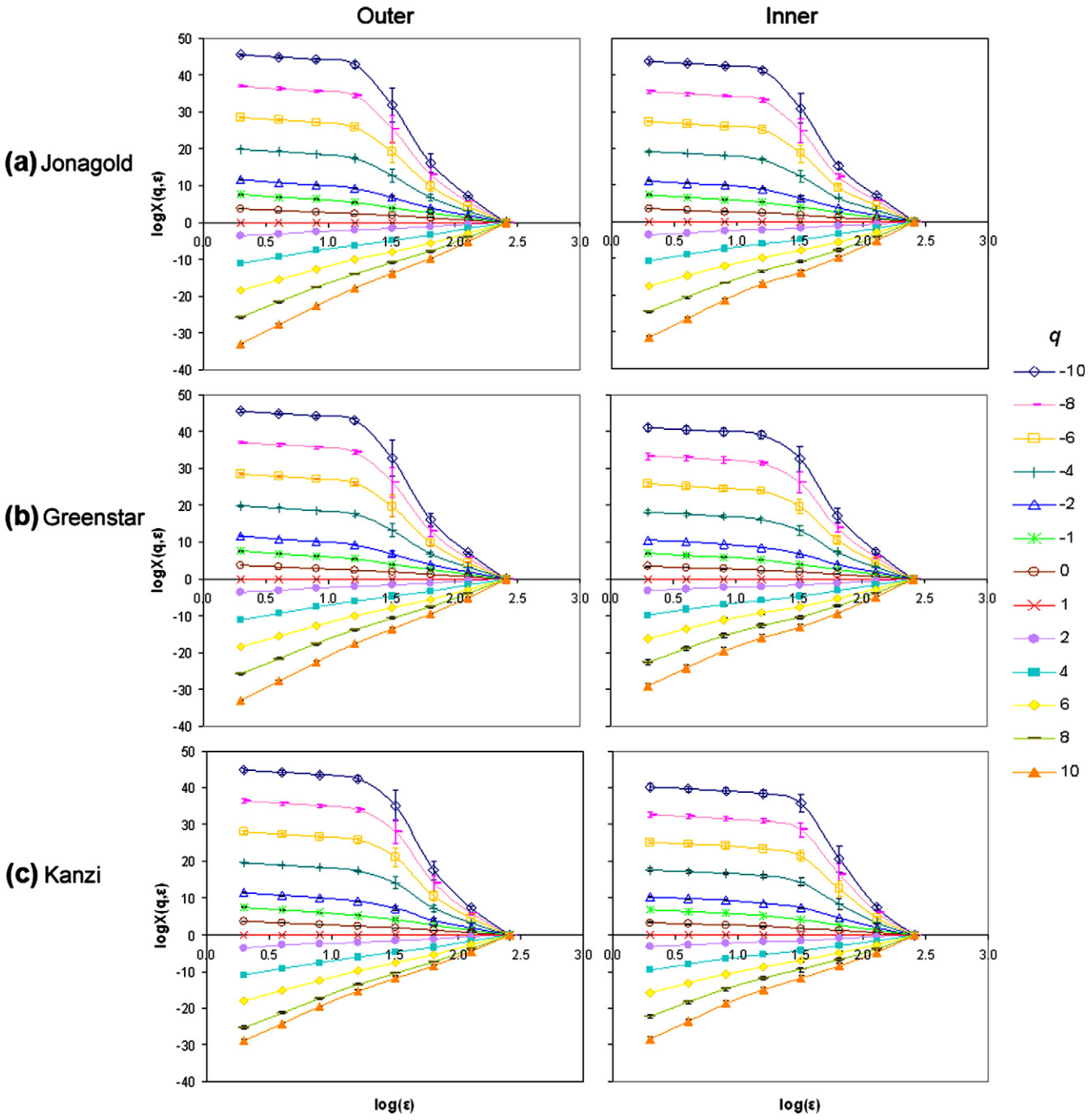

Fig. 2. The partition function of all images for $-10 \leqslant q \leqslant 10$ over box sizes ε ranging from 2 to 256 pixels. The mass exponent τ is estimated as the slope of the log/log data for the *outer* and *inner* pore space.

changes of D_0, D_1 andD_2 in the same spectra for all cultivars and positions revealed significant differences among them ($p < 0.05$). The standard deviations given in Table 2 correspond to two replicates with 600 images per repetition extracted from the same apple. In general, they were constant in the evaluated range (D_0 to D_2). The smallest standard deviation was for D_0 of *outer* tissue of *Jonagold* (±0.017), and the highest was for D_2 of *inner* tissue of *Greenstar* (±0.050).

The main distinction between all images is the difference between D_0 and D_2 or $D_0 - D_2$ which allowed to statistically differentiate and characterize both positions and al three cultivars ($p < 0.05$). The values of $D_0 - D_2$ are larger for *inner* tissue than for *outer* tissue. The largest difference (0.090 ± 0.006) was found for *Greenstar* and the smallest one for *Jonagold* (0.072 ± 0.004). In the *outer* tissue, however, although the range of $D_0 - D_2$ was smaller (0.051 ± 0.004 to 0.056 ± 0.005), statistical differences were found among cultivars ($p < 0.05$). In addition, the heterogeneity of the PSD of apple tissue was quantified by obtaining the ratio of the two parameters D_1/D_0. This relation allowed studying the dispersion of the porosity with respect to the pore-size since it provides information about the proportional variation instead of the absolute variation, similar to, for example, a coefficient of variation in statistics. This ratio was the largest for the *outer* tissue in all cultivars ($\sim 0.979 \pm 0.002$) but no significant differences were

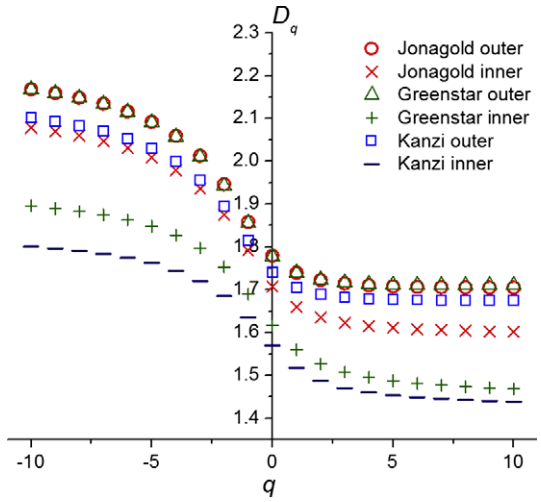

Fig. 3. Generalized dimensional spectra for the images of apple tissue extracted from *outer* and *inner* regions.

observed. For the *inner* images *Jonagold* was significantly different from both other cultivars.

5. Discussion

Multifractal spectra are graphs of how a pattern behaves if amplified in certain ways. The algorithms implemented for the purpose of this article generate a mass distribution for an image and make graphs of D_q vs. q and of τ, which are all variously called multifractal spectra.

The D_q addresses how mass varies with ε (resolution or box size) in an image (FracLab, 2003). Multifractal spectra can be considered as fingerprints characterizing fractal objects; differences in a multifractal spectrum imply a different fractal structure which may affect processes such as gas exchange in the fruit.

Generalized dimensions D_q have been obtained with the method of moments for the multiscale analysis of the PSD of three different apple cultivars in two positions of the parenchyma tissue (near the peel and near the core). The generalized dimensional spectra illustrate that the PSD in apple tissue has multifractal characteristics. The heterogeneity in the porosity distribution among cultivars was visually evident from the 2-D images shown in Fig. 1, and it was possible to quantitatively determine their scaling properties and microstructural differences in relation to their PSD spectrum. These results provide a picture of how the pore structure of apple tissue can vary between cultivars. The PSD analysis using D_q parameters suggested that the porosity in each apple cultivar is distributed according to a power-law distribution whose exponents also showed to be able to differentiate between the cultivars and also between different regions of the same cultivar. The multifractal parameters may be used to differentiate between the pore microstructure and size-distributions of apple cultivars.

This is the first time that multifractal algorithms have been used to characterize the variability of PSD in apple tissue at micron resolution. The motivation for the use of multifractal analysis rests on the origin of this mathematical tool, which is to characterize the hidden order in apparently random signals of distributions coming from chaotic deterministic systems or from random processes (Halsey et al., 1986; Lévi Véhel, 1996). The quantitative characterization and modeling of apple microstructure based on multifractal analysis is a novel approach to improve our understanding of how the microstructure affects physiological processes and mechanical behavior of the fruit during postharvest processes such as low temperature storage, packing and trading. In addition, X-ray image technology allowed a real representation of the internal structure of the apple matrix, and therefore, a better visualization and understanding of the pore organization and complexity of the sample.

Multifractal formalisms are not simple for implementation and define. In this study, the success in getting well-defined and differentiated generalized dimensional spectra among apple cultivars can be mainly attributed to two factors. First, we extracted information from images captured with a spatial resolution of 8.5 μm/pixel and field of view of 4.74 mm^2 (256×256 $pixels^2$) which could be considered as representative areas for analysis of PSD in apple tissue. Our previous investigations (Mendoza et al., 2007) using *Jonagold* apples have shown, based on porosity measurements, that there is a critical resolution around 13.7 μm/pixel which could be used as the upper limit for suitable geometrical measurements in apple tissue using X-ray micro-CT. Secondly, taking advantage of the symmetric shape of the apples, we used average information gathered from two opposite sides of the same fruit for each analyzed region and cultivar (600 slices per sample), increasing the precision in the regression analysis for slope estimation (D_q values).

However, it is important to mention that the sensitivity of the multifractal analysis based on image analysis is strongly dependent on the size of the image. Digital images always have a limited size (number of pixels), and only a few pixels can cause great changes in the partition function especially for negative moment q. In this study, we used images with size of 256×256 pixels and in Table 1 and Fig. 2 it should be noted that for negative values, the coefficients of determination (R^2) decreased from 0.982 ($q = -1$) for *outer* tissue in *Jonagold* apples to 0.812 ($q = -10$) for *inner* tissue in *Kanzi* apples. When the slope of $\log(X(q,\varepsilon))$ over $(\log \varepsilon)$ does not yield a straight line for all ε, different generalized dimensions will be obtained for specific values of ε. Therefore, this should be checked and carefully considered for interpretation of the data. In this respect, we have determined in our previous investigations (Mendoza et al., 2007) that the minimum representative elementary volume (REV) for a continuum assumption of porosity in apple tissue is around of 1.3 mm^3 (equivalent to 128 pixels/side using a resolution of 8.5 μm/pixel) which has showed a reasonable standard deviation of 2.7% for porosity using 12 sub-volumes from 3 apple samples and an estimated standard error of 0.7%. The REV is defined as the range of volumes over which a statistical average can be performed (Bear, 1972).

Data of apple microstructure exhibit great complexity that spatial analyses try to understand. Representation of the 3-D percolating backbone (skeleton) of parenchyma pore space of *Jonagold* apple (near to the peel) and synchrotron microtomography images (Verboven et al., 2008) has revealed that the intercellular space is highly interconnected and forms a complicated network inside the tissue (Mendoza et al., 2007). Therefore, apple flesh cannot be regarded as a homogeneous material (Mebatsion et al., 2006a,b). The differences in the size, orientation, and organization of the air channels strongly contribute to the anisotropy and heterogeneity of apple flesh (Khan and Vincent, 1990, 1993a; Vincent, 1989). The implications of anisotropy of apple flesh are wide ranging; it has been frequently assumed to contribute to the particular textural properties of each fruit (Khan and Vincent, 1990, 1993b). The PSD has a critical influence on transport properties such as permeability, and its quantification is important for understanding microstructure–transport property relationships (Celia et al., 1995; Dražeta et al., 2004; Ho et al., 2009). We found that apple samples from different cultivars and position in the same cultivar differ in PSD, and therefore, in their scaling properties. D_q values of pore structure at different positions but for the same apple cultivar have similar

tendencies, but are different in width which gives information of the heterogeneity of the PSD in the samples.

Porosity analysis of the three apple samples and parenchyma regions confirmed the pore-size differences appreciated in Fig 1. Also, analysis revealed high correlations between the parameters D_0, D_1 and D_2 and porosity measurements ($R^2 \geqslant 0.971$, Fig. 4) for all these apple samples. However, it is important to note here that bulk porosity measurements and even D_0 do not provide information about the scaling properties of a pore structure. Calculation of D_0 assumes a homogeneous apple tissue structure (i.e., at every partition level, all the boxes have the same probability). Similarly, both $D_0 - D_2$ and D_1/D_0 showed high correlations with porosity measurements. The implication of this finding is that the PSD of apple tissue can be characterized almost entirely by the generalized dimensions and relations. However, this interpretation needs to be weighted by considering that apple tissue was analyzed using a stack of images separated 8.5 μm with a depth of 5.1 mm.

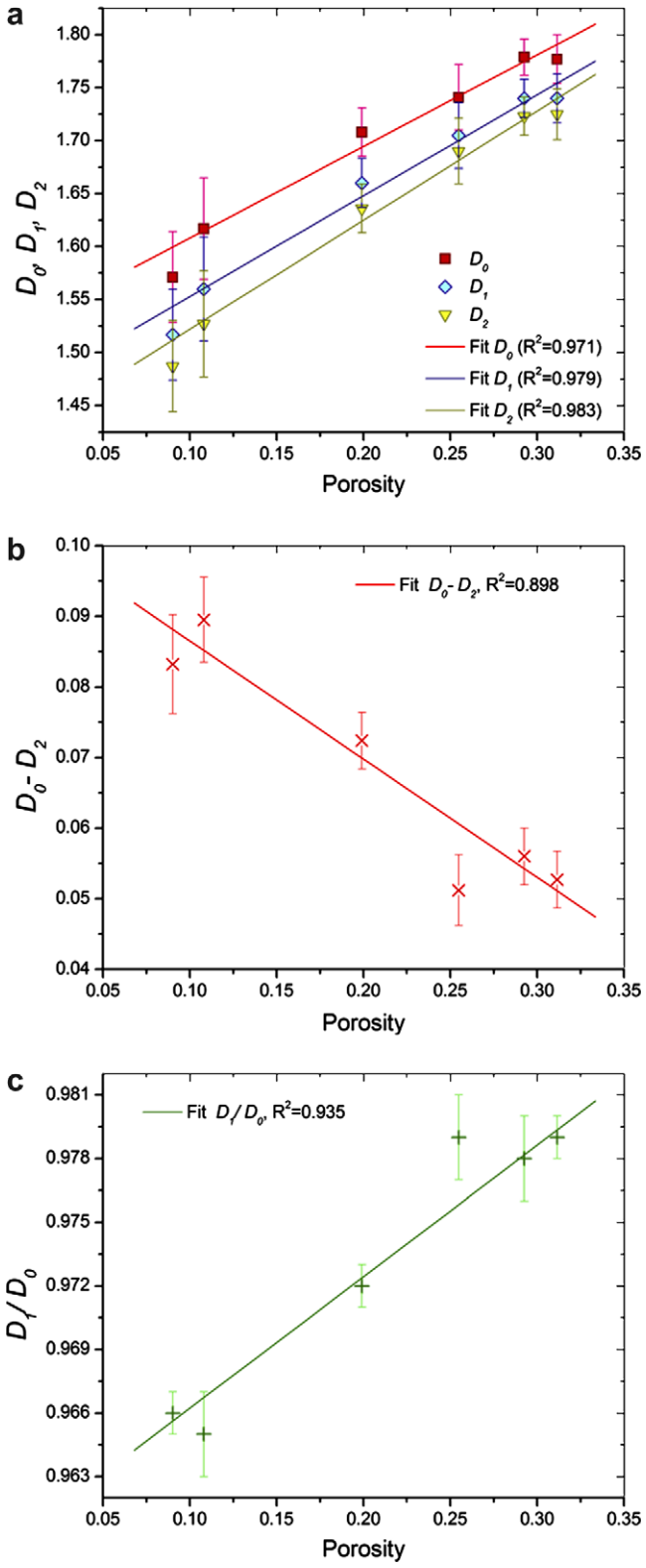

Fig. 4. Correlations between multifractal parameters and porosity measurements of apple tissue. (a) for D_0, D_1 and D_2, (b) $D_0 - D_2$, and (c) D_1/D_0.

As seen in Fig. 3 and Table 2, the estimated Rényi parameters D_0, D_1 and D_2 from 2-D cross-section images at micron resolution allow for characterization of multiscaling properties among other features based on the PSD of apple tissue. Of particular interest is the correlation dimension D_2 which not only showed the highest correlation with porosity ($R^2 = 0.983$, Fig. 4a), but also because when used in the difference $D_0 - D_2$ statistical differences ($p < 0.05$) among all apple PSD's (Table 2) are found. It is notable since the *outer* tissue structures from *Jonagold* and *Greenstar* apples are difficult to differentiate using the other Rényi parameters (Table 2). Nonetheless, the observed correlation coefficient between $D_0 - D_2$ and porosity was the lowest one ($R^2 = 0.898$) in comparison with the other evaluated multifractal parameters ($D_0, D_1, D_2,$ and D_1/D_0) (Fig. 4).

The results of this study have also demonstrated that multifractal analysis has significant benefits for the quantitative analysis of the complex microstructure of apple images, allowing conclusions to be drawn on the exact topography of the PSD of apple tissue. This multiscaling procedure and image analysis technique should provide valuable opportunities for further research in other fruits plants and vegetables.

Finally, it is important to note that food engineers and food researchers currently need novel experimental tools and analysis methods based on physical or mathematical models to describe the PSD in a quantitative way. This may help in improving our understanding how the PSD affects food processes such as heat and mass transfer or mechanical behavior. A number of articles have been published on the basic concepts of fractal analysis such as box-counting method (Rahman, 1997; Quevedo et al., 2002; Alamilla-Beltrán et al., 2005) or the Fourier fractal method (Quevedo et al., 2008, 2009) applied to food engineering problems. The multifractal analysis proposed in this article is a step forward as it presents a better method to describe the PSD of foods. Multifractal analysis is founded on physical concepts that are well accepted and used in many other areas of engineering and research. The method can easily be applied to other porous foods.

6. Conclusions

Multifractal parameters were found to reflect the major aspects of variability in the pore-scale of apple tissue, and provided a unique quantitative characterization of the data spatial distribution. The irregularity and complexity of apple pore structure, together with its scale-invariant features suggest that a multifractal distribution is a suitable and natural model. In this paper, generalized dimensions of apple pore structure are computed for data obtained from 2-D X-ray images at resolution of 8.5 μm, obtained from the *outer* and *inner* regions of three apple cultivars. The multifractal generalized spectrum can be used advantageously to describe the scaling properties of the heterogeneous porosity distribution in apple parenchyma tissue. The variation of D_q with respect to q and the shape of the generalized dimension spectrum reveal that the PSD structure of apple tissue has properties close to multifractal self-similarity measures; generalized dimensions D_q successfully

characterized the PSD and the heterogeneity of the apple tissue structure. The value of $D_0 - D_2$ were found to have a suitable discriminatory ability for studying the PSD heterogeneity of apple tissue. These results show that multifractal generalized dimensional analysis is an appropriate tool for characterizing the heterogeneity of pore space structure in apple fruit. A further step would be to correlate such generalized dimensions to physical properties of the fruit such as its gas transport properties or mechanical properties. In this way microscale physical properties of the fruit which are almost impossible to measure at this scale could be inferred based on the multifractal characteristics of the microstructure.

The multifractal generalized dimensional analysis such as reported in this manuscript can also be applied to other porous foods such as cookies.

Acknowledgements

The authors wish to thank to K.U. Leuven (Project OT 04/31) and the Fund for Scientific Research Flanders (F.W.O. – Vlaanderen, Project G.0200.02) for financial support for this investigation.

References

Alamilla-Beltrán, L., Chanona-Pérez, J.J., Jiménez-Aparicio, A.R., Gutierrez-López, G.F., 2005. Description of morphological changes of particles along spray drying. Journal of Food Engineering 67, 179–184.

Baoping, J., 1999. Nondestructive technology for fruits grading. In: Proceedings of 99 International Conference on Agricultural Engineering, Beijing, China, December, pp. IV127–IV133.

Baumann, H., Henze, J., 1983. Intercellular space volume of fruit. Acta Horticulturae 138, 107–111.

Bear, J., 1972. Dynamics of Fluids in Porous Media. Dover Publishing Co., New York.

Celia, M., Reeves, P., Ferrand, L., 1995. Recent advances in pore scale models for multiphase flow in porous media. Reviews of Geophysics Supplement 33, 1049–1057.

Cheng, Q., Banks, N.H., Nicholson, S.E., Kingsley, A.M., Mackay, B.R., 1998. Effects of temperature on gas exchange of 'Braeburn' apples. New Zealand Journal of Crop and Horticultural Science 26, 299–306.

Chhabra, A., Jensen, R.V., 1989. Direct determination of the $f(\alpha)$ singularity spectrum. Physical Review Letters 62 (12), 1327–1330.

Cox, L.B., Wang, J.S.Y., 1993. Fractal surfaces: measurements and applications in earth sciences. Fractals 1, 87–117.

Dathe, A., Tarquis, A.M., Perrier, E., 2006. Multifractal analysis of pore- and solid-phases in binary two-dimensional images of natural porous structures. Geoderma 134, 318–326.

De Smedt, V., Pauwels, E., De Baerdemaeker, J., Nicolaï, B.M., 1998. Microscopic observation of mealiness in apples: a quantitative approach. Postharvest Biology and Technology 14, 151–158.

Dražeta, L., Lang, A., Alistair, J.H., Richard, K.V., Paula, E.J., 2004. Air volume measurement of 'Braeburn' apple fruit. Journal of Experimental Botany 55, 1061–1069.

Eghball, B., Schepers, J.S., Negahban, M., Schlemmer, M.R., 2003. Spatial and temporal variability of soil nitrate and corn yield: multifractal analysis. Agronomy Journal 95, 339–346.

Esau, K., 1977. Anatomy of Seed Plants, second ed. John Wiley and Sons, New York.

Evertsz, C.J.G., Mandelbrot, B.B., 1992. Multifractal measures. In: Peitgen, H., Jürgens, H., Saupe, D. (Eds.), Chaos and Fractals. Springer, Berlin, pp. 922–953.

Feder, J., 1988. Fractals. Plenum Press, New York.

FracLab, 2003. Notes on the generalized dimension spectrum and multifractality. FracLac for ImageJ. URL: <http://www.geocities.com/akarpe@sbcglobal.net/multifract.html>.

Franck, C., Lammertyn, J., Ho, Q.T., Verboven, P., Verlinden, B.E., Nicolai, B.M., 2007. Browning disorders in pear fruit. Postharvest Biology and Technology 43, 1–13.

Gonzales-Barron, U., Butler, F., 2008. Fractal texture analysis of bread crumb digital images. European Food Research And Technology 226, 721–729.

Grassberger, P., Procaccia, I., 1983. Characterization of strange attractors. Physical Review Letters 50, 346–349.

Hagiwara, T., Wang, H.L., Suzuki, T., Takai, R., 2002. Fractal analysis of ice crystals in frozen food. Journal Of Agricultural And Food Chemistry 50, 3085–3089.

Halsey, T.C., Jensen, M.H., Kadanoff, L.P., Procaccia, I., Shraiman, B.I., 1986. Fractal measures and their singularities: the characterization of strange sets. Physical Review A 33 (2), 1141–1151.

Harker, F.R., Ferguson, I.B., 1988. Calcium ion transport across discs of the cortical flesh of apple fruit in relation to fruit development. Physiol Plant 74, 695–700.

Harker, F.R., Hallet, I.C., 1992. Physiological changes associated with development of mealiness of apple fruit during cool storage. HortScience 27, 1291–1294.

Harker, F.R., Watkins, C.B., Brookfield, P.L., Miller, M.J., Reid, S., Jackson, P.J., Bieleski, R.L., Bartley, T., 1999. Maturity and regional influences on watercore development and its postharvest disappearance in 'Fuji' apples. Journal of the American Soil Science Society 124, 166–172.

Hentchel, H.G.E., Procaccia, I., 1983. The infinite number of generalized dimensions of fractals and strange attractors. Physica D 8, 435–444.

Ho, Q.T., Verlinden, B.E., Verboven, P., Nicolaï, B.M., 2006. Gas diffusion properties at different positions in the pear. Postharvest Biology and Technology 41, 113–120.

Ho, Q.T., Verboven, P., Verlinden, B.E., Lammertyn, J., Vandewalle, S., Nicolaï, B.M., 2008. In: A continuum model for gas exchange in pear fruit. PLOS Computational Biology 4 (3), e1000023.

Ho, Q.T., Verboven, P., Mebatsion, H.K., Verlinden, B.E., Vandewalle, S., Nicolaï, B.M., 2009. Microscale mechanisms of gas exchange in fruit tissue. New Phytologist. doi:10.1111/j.1469-8137.2008.02732.x.

Ho, Q.T., Verboven, P., Verlinden, B.E., Schenk, A., Rolletschek, H., Vercammen, J., Nicolaï, B.M., 2010. Genotype effects on internal gas gradients in apple fruit. Journal of Experimental Botany, submitted for publication.

Kerdpiboon, S., Devahastin, S., Kerr, W.L., 2007. Comparative fractal characterization of physical changes of different food products during drying. Journal Of Food Engineering 83, 570–580.

Ketipearachchi, K.W., Tatsumi, J., 2000. Local fractal dimensions and multifractal analysis of the root system of legumes. Plant Production Science 3, 289–295.

Khan, A.A., Vincent, J.F.V., 1990. Anisotropy of apple parenchyma. Journal of the Science of Food and Agriculture 52, 455–466.

Khan, A.A., Vincent, J.F.V., 1993a. Compressive stiffness and fracture properties of apple and potato parenchyma. Journal of Texture Studies 24, 423–435.

Khan, A.A., Vincent, J.F.V., 1993b. Anisotropy in the fracture properties of apple flesh as investigated by crack-opening tests. Journal of Materials Science 28, 45–51.

Korvin, G., 1992. Fractals Models in the Earth Sciences. Elsevier, Amsterdam.

Kravchenko, A.N., Boast, C.W., Bullock, D.G., 1999. Multifractal analysis of soil variability. Agronomy Journal 91, 1033–1041.

Kuroki, S., Oshita, S., Sotome, I., Kawagoe, Y., Seo, Y., 2004. Visualization of 3-D network of gas-filled intercellular spaces in cucumber fruit after harvest. Postharvest Biology and Technology 33, 255–262.

Lévi Véhel, J., 1996. Fractal approaches in signal processing. In: Evertsz, C.J.G., Peitgen, H.O., Voss, R.F. (Eds.), Fractal Geometry and Analysis. The Mandelbrot Festschrift, Curacao 1995. World Scientific Singapore.

Machs, J., Mas, F., Sagues, F., 1995. Two representations in multifractal analysis. Journal of Physics A: Mathematics and General 28, 5607–5622.

Mandelbrot, B.B., 1989. The Fractal Geometry of Nature. Freeman, San Francisco.

Mardia, K.V., Hainsworth, T.J., 1988. A spatial thresholding method for image segmentation. IEEE Transactions on Pattern Analysis and Machine Intelligence 6, 919–927.

Mebatsion, H.K., Verboven, P., Verlinden, B.E., Ho, Q.T., Nguyen, T.A., Nicolaï, B., 2006a. Microscale modeling of fruit tissue using Voronoi tessellations. Computers and Electronics in Agriculture 52, 36–48.

Mebatsion, H.K., Verboven, P., Ho, Q.T., Mendoza, F., Verlinden, B.E., Nguyen, T.A., Nicolaï, B., 2006b. Modeling fruit microstructure using novel ellipse tessellations algorithm. Computer Modeling in Engineering and Science 14, 1–14.

Mendoza, F., Verboven, P., Ho, Q.T., Mebatsion, H.K., Nguyen, T.A., Webers, M., Nicolaï, B.M., 2006. 3-D Microscale geometry of apple tissue using X-ray computed microtomography. In: Proceedings of IUFoST 13th World Congress of Food Sciences and Technology, FOOD IS LIFE, Nantes, France.

Mendoza, F., Verboven, P., Mebatsion, H.K., Kerckhofs, G., Wevers, M., Nicolaï, B.M., 2007. Three-dimensional pore space quantification of apple tissue using X-ray computed microtomography. Planta 226, 559–570.

Oh, W., Lindquist, W., 1999. Image thresholding by indicator kriging. IEEE Transactions on Pattern Analysis and Machine Intelligence 21, 590–602.

Pascual, M., Ascioti, F.A., Caswell, H., 1995. Intermittency in the plankton: a multifractal analysis of zooplankton biomass variability. Journal of Plankton Research 17, 1209–1232.

Plotnick, R.E., Gardner, R.H., Hargrove, W.W., Prestegaard, K., Perlmutter, M., 1996. Lacunarity analysis: a general technique for the analysis of spatial patterns. Physical Review E 53 (5), 5461–5468.

Posadas, A., Giménez, D., Quiroz, R., Protz, R., 2003. Multifractal characterization of soil pore systems. Journal of the American Soil Science Society 65, 1361–1369.

Quevedo, R., López-G, C., Aguilera, J.M., Cadoche, L., 2002. Description of food surfaces and microstructural changes using fractal image texture analysis. Journal of Food Engineering 53, 361–371.

Quevedo, R., Mendoza, F., Aguilera, J.M., Chanona, J., Gutiérrez-López, G., 2008. Determination of senescent spotting in banana (*Musa cavendish*) using fractal texture Fourier image. Journal of Food Engineering 53, 361–371.

Quevedo, R., Jaramillo, M., Diaz, O., Pedreschi, F., Aguilera, J.M., 2009. Quantification of enzymatic browning in apple slices applying the fractal texture Fourier image. Journal of Food Engineering 95, 285–290.

Rahman, M.S., 1997. Physical meaning and interpretation of fractal dimensions of fine particles measured by different methods. Journal of Food Engineering 32, 447–456.

Rajapakse, N.C., Banks, N.H., Hewett, E.W., Cleland, D.J., 1990. Development of oxygen concentration gradients in flesh tissues of bulky plant organs. Journal of the American Society for Horticultural Science 115, 793–797.

Raven, J.A., 1996. Into the voids: the distribution, function, development and maintenance of gas spaces in plants. Annals Botany 78, 137–142.

Rényi, A., 1995. On a new axiomatic theory of probability. Acta Mathematica Hungarica VI (3–4), 285–335.

Scheuring, I., Riedi, R.H., 1994. Application of multifractals to the analysis of vegetation pattern. Journal of Vegetation Science 5, 489–496.

Shannon, C.E., Weaver, W., 1949. The Mathematical Theory of Communication. University of Illinois Press, Chicago.

Tang, D.M., Marangoni, A.G., 2008. Fractal dimensions of simulated and real fat crystal networks in 3D space. Journal Of The American Oil Chemists Society 85, 495–499.

Tu, K., De Baerdemaeker, J., Deltour, R., de Barsy, T., 1996. Monitoring post-harvest quality of Granny Smith apple under simulated shelf-life conditions: destructive, non-destructive and analytical measurements. International Journal of Food Science and Technology 31, 267–276.

Verboven, P., Kerckhofs, G., Mebatsion, H.K., Ho, Q.T., Temst, K., Wevers, M., Cloetens, P., Nicolaï, B.M., 2008. 3-D gas exchange pathways in pome fruit characterized by synchrotron X-ray computed tomography. Plant Physiology 147, 518–527.

Vincent, J.F.V., 1989. Relationships between density and stiffness of apple flesh. Journal of the Science of Food and Agriculture 31, 267–276.

Vicsek, T., 1992. Fractal Growth Phenomena, second ed. Word Scientific Publishing Co., Singapore.

Voss, R.F., 1988. Fractals in nature: From characterization to simulation, In: Peitgen, H., & Saupe, D. (Eds.), The sciences of Fractal Images. Springer, New York, pp. 21–69.

Volz, R.K., Harker, F.R., Hallet, I.C., Lang, A., 2004. Development of texture in apple fruit – a biophysical perspective. Acta Horticulturae 636, 473–479.

Westwood, M.N., Batjer, L.P., Billingsley, H.D., 1967. Cell size, cell number and fruit density of apples as related to fruit size, position in the cluster and thinning method. Proceedings of the American Society for Horticultural Science 91, 51–62.

Xiaoyan, G., Peiling, Y., Shumei, R., Yunkai, L., 2007. Multifractal analysis of soil structure under long-term wastewater irrigation based on digital image technology. New Zealand Journal of Agricultural Research 50, 789–796.

Yamaki, S., Ino, M., 1992. Alteration of cellular compartmentation and membrane permeability to sugars in immature and mature apple fruit. Journal of the American Society for Horticultural Science 117, 951–954.

Yearsley, C.W., Banks, N.H., Ganesh, S., 1997a. Temperature effects on the internal lower oxygen limits of apple fruit. Postharvest Biology and Technology 11, 73–83.

Yearsley, C.W., Banks, N.H., Ganesh, S., 1997b. Effects of carbon dioxide on the internal lower oxygen limits of apple fruit. Postharvest Biology and Technology 12, 1–13.